Title

Colloid Deposit Morphology and Clogging in Porous Media: Fundamental Insights Through Investigation of Deposit Fractal Dimension

Journal

Environmental Science and Technology, 49(20)

ISSN

0013-936X

Authors

Roth, Eric J
Gilbert, Benjamin
Mays, David C

Publication Date

2015-10-20

DOI

10.1021/acs.est.5b03212

Peer reviewed

Colloid Deposit Morphology and Clogging in Porous Media: Fundamental Insights Through Investigation of Deposit Fractal Dimension

Eric J. Roth[†], Benjamin Gilbert[‡], and David C. Mays[*†]

[†] University of Colorado Denver, Department of Civil Engineering, Campus Box 113, PO Box 173364, Denver, Colorado 80217-3364, United States

[‡] Lawrence Berkeley National Laboratory, Earth Sciences Division, Mail Stop 74R316C, 1 Cyclotron Road, Berkeley, California 94720, United States

*Phone 303-352-3933; e-mail david.mays@ucdenver.edu.

Publication Date (Web): September 27, 2015

DOI: 10.1021/acs.est.5b03212

Abstract

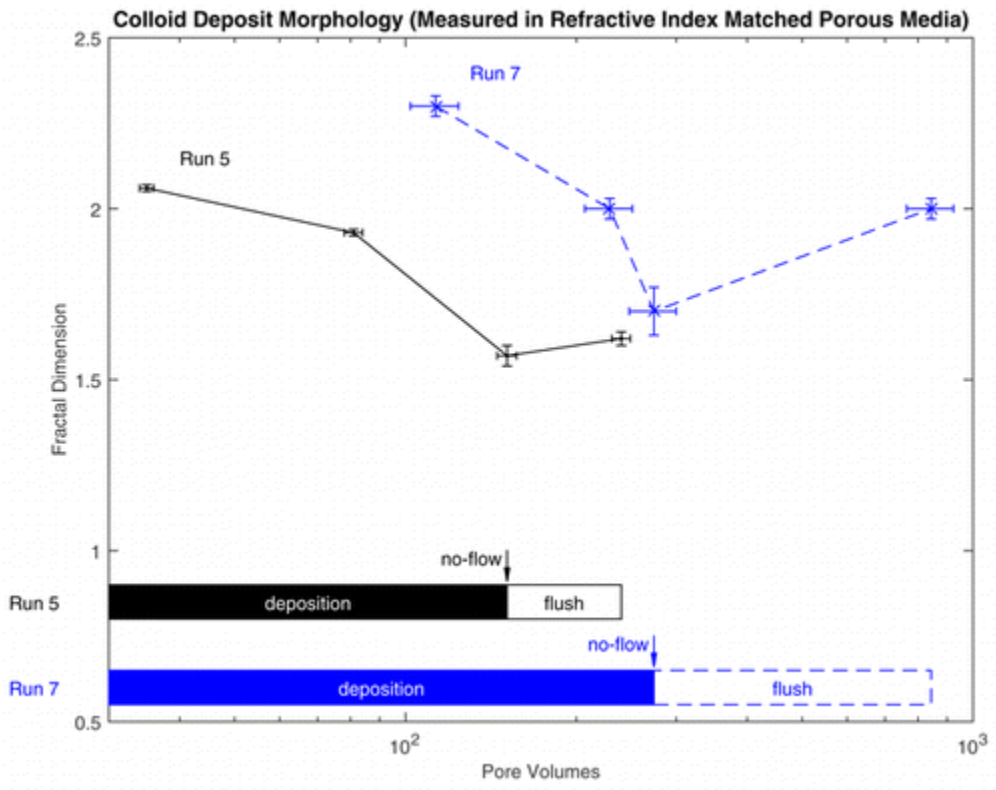

Experiments reveal a wide discrepancy between the permeability of porous media containing colloid deposits and the available predictive equations. Evidence suggests that this discrepancy results, in part, from the predictive equations failing to account for colloid deposit morphology. This article reports a series of experiments using static light scattering (SLS) to characterize colloid deposit morphology within refractive index matched (RIM) porous media during flow through a column. Real time measurements of permeability, specific deposit, deposit fractal dimension, and deposit radius of gyration, at different vertical positions, were conducted with initially clean porous media at various ionic

strengths and fluid velocities. Decreased permeability (i.e., increased clogging) corresponded with higher specific deposit, lower fractal dimension, and smaller radius of gyration. During deposition, fractal dimension, radius of gyration, and permeability decreased with increasing specific deposit. During flushing with colloid-free fluid, these trends reversed, with increased fractal dimension, radius of gyration, and permeability. These observations suggest a deposition scenario in which large and uniform aggregates become deposits, which reduce porosity, lead to higher fluid shear forces, which then decompose the deposits, filling the pore space with small and dendritic fragments of aggregate.

Introduction

The equation created by Josef Kozeny(1) and modified by Philip Carman(2) is the most common approach for estimating the permeability of porous media. In its simplest form, the Kozeny-Carman equation expresses permeability, k, as a function of porosity, n, and median grain size, d_{50}:

$$k = \frac{n^3}{(1-n)^2}\frac{{d_{50}}^2}{180} \quad (1)$$

Equation 1 works well for single phase flow in approximately monodisperse porous media, in which the empirical factor is 180 as shown above.(3) However, in applications where the pore space geometry is complicated by colloid deposition, mineral precipitation, or biofilm growth, the Kozeny-Carman equation overestimates permeability by multiple orders of magnitude.(4) It has been known for some time that the introduction or mobilization of fine particles in soils with diameters between 10^{-9} and 10^{-5} m (i.e., colloidal particles) can cause large reductions in soil permeability.(5) However, the relationships between the colloidal properties of soil fines, the mechanism of permeability change, and soil function are still being investigated.(4, 6-11) In particular, numerous studies have demonstrated that knowing the volume of deposited colloids per volume of porous media (i.e., specific deposit) does not allow prediction of permeability, because even when the specific deposit is held constant, permeability can vary by orders of magnitude.(12-15) These studies suggest that deposit morphology, defined as the geometric arrangement of colloids within the pore space, has important effects on permeability.

Deposit morphology can be quantified using two standard metrics in colloid science, fractal dimension and radius of gyration (Figure 1). The fractal dimension is a measure of geometric complexity as a function of scale:(16-18)

$$N = \beta\left(\frac{R_g}{r}\right)^D \quad (2)$$

where N is the number of colloids per deposit, R_g is the radius of gyration, r is the colloid diameter, β is a proportionality constant, and D is the fractal dimension. When D = 1, the number of colloids N is proportional to size expressed as a dimensionless radius R_g/r; when D = 2, N is proportional to size squared; when D = 3, N is proportional to size cubed. These number-size relationships, or equivalently mass-length relationships, correspond to 1-, 2-, and 3-dimensional objects, respectively. The fractal dimension D generalizes these scaling relationships to noninteger values, which has allowed the description of numerous natural observations in a mathematical framework.(16) In principle, fractals have no characteristic length scale. However, for colloid aggregates, a lower size limit is imposed by the diameter of the primary colloids, and an

upper size limit is imposed by the overall size of the deposit, so accordingly one can define a characteristic size, which is taken to be the radius of gyration. The radius of gyration is the root mean squared distance of aggregate elements from the aggregate center of mass. That is, if the colloids shown in any panel of Figure 1 were rearranged into a hollow spherical shell with identical moment of inertia, the radius of gyration would be the radius of the hollow spherical shell. Accordingly, radius of gyration is a convenient metric to describe the characteristic size of irregularly shaped colloid deposits.

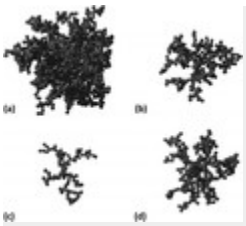

Figure 1. Conceptual illustrations of colloid deposit morphology using measured *D*and R_g for the middle region of experiment 7. (a) early deposition phase with D = 2.3, R_g = 1034 nm, and Pore Volumes Eluted (PV) = 113; (b) late deposition phase with D = 2.0, R_g = 771 nm, PV = 229; (c) no-flow phase with D = 1.7, R_g = 673 nm, PV = 274; and (d) flushing phase with D = 2.0, R_g = 840 nm, PV = 844. Illustrations generated with DLA Version 1.13.02.(46)

Over the last 10–20 years, the morphology of colloid aggregates or deposits has been shown to play important roles in colloid transport, nanoparticle reactivity, and particle removal by settling and filtration.(19) Extensive research has been (and continues to be) devoted to colloid transport in porous media,(20-23) including several recent studies that have sought to correlate colloid transport with aggregate morphology measured by static light scattering (SLS) for suspended colloid aggregates. For example, Lin and Wiesner(24) investigated the affinity between nanoparticles and flat surfaces, concluding that the size of the individual colloids control the attachment efficiency, rather than the size of the aggregate. Chowdhury et al. (25) quantified aggregate morphology of titanium dioxide nanoparticles using fractal dimension and hydrodynamic radius, which is analogous to the radius of gyration, concluding that aggregate morphology controls environmental transport of nanoparticles. In particular, they observed that aggregates with smaller fractal dimensions are more susceptible to breakup during transport through porous media and therefore manifest increased mobility. Jassby et al.(26) also quantified aggregate morphology using fractal dimension and hydrodynamic radius, concluding that the aggregate morphology of titanium dioxide nanoparticles and zinc oxide nanoparticles determines not just their environmental transport, but also their reactivity. Legg et al.(27) investigated the effect of ionic strength on aggregate formation, finding that ferrihydrite nanoparticles in the absence of salt formed low-density fractal aggregates with resilient structures that resisted collapse and exhibited little deposition in a sand filled column. Upon addition of sodium nitrate, aggregates would collapse into dense structures, exhibiting high rates of deposition. None of these studies were able to directly probe the morphology of the aggregates inside the porous medium.

In parallel, aggregate morphology has been shown to influence colloid removal by settling, and deposit morphology has been shown to influence permeability during colloid removal by filtration. Theoretical research linking aggregate morphology and settling velocity is ongoing,(28) and there are numerous examples in the literature. For example, simulations by Xu and Fan(29) indicate that colloid aggregates with lower fractal dimensions have faster settling velocity. Fellay et al.(30)noted that fluid flow influences aggregate morphology, and went on to highlight the feedback process whereby colloid aggregates influence flow in porous media. Other similar feedback processes have been identified, showing that flow in porous media both controls and depends on mineral precipitation,(31) growth of biomass,(32) and in situ bioremediation.(33) Indeed, this

feedback between flow and deposition is at the heart of filtration dynamics, and was the subject of pioneering simulations(34) and experiments(15) in the 1990s. In particular, Veerapaneni and Wiesner(15) explored the hypothesis that colloid deposit morphology could be quantified as a fractal dimension, which they measured ex situ after resuspending frozen deposits extracted destructively. Furthermore, the link between deposit morphology and permeability is also relevant to membrane filtration, giving due attention to the qualitative differences between clogging in granular media filters and membrane filters.(9) For example, Wang et al.(35) used scanning electron microscopy to show that large aggregates with high fractal dimension had higher permeability. These results compliment the numerical simulations by Ghezzehei,(4) who found that deposit morphology was essential for predicting the permeability of porous media after mineral precipitation or biofilm growth.

Thus, there is growing indirect evidence implicating colloid deposit morphology as a key factor affecting permeability and indicating that that fractal dimension could be a suitable metric. Although fractal dimension is routinely measured for colloidal suspensions in bulk fluids,(17, 18, 36-38) no experimental technique has been available to measure colloid deposit morphology with voxel resolution of 50 nm or less within porous media in real time. Direct imaging methods currently lack the spatial resolution to determine deposit morphology of submicron colloids within a pore network.

We developed an approach using static light scattering (SLS) to characterize the fractal dimension of colloidal aggregates in refractive index matched (RIM) porous media.(39, 40) Here, our objectives are (1) to extend this approach to study real-time clogging processes, and (2) to summarize the results of a suite of experiments studying the flow and deposition of 106 nm diameter carboxylate-modified polystyrene microspheres in a saturated column containing Nafion grains. SLS was chosen over other imaging techniques, such as X-ray microtomography,(6, 7, 11)due in part to the small length scales it can characterize. The experimental conditions span a range of salt concentrations, flow rates and flow regimes. Although the colloidal particles and porous medium are not environmental materials, they enable new insights into deposition processes and permeability reduction that is relevant to a wide range of natural and engineered systems.

Materials and Methods

Using the apparatus described in Roth et al.,(40) the porous media used for experiments was 16–35 mesh granular Nafion (C.G. Processing, Rockland, DE), a fluorinated ionomer for which refractive index matching is possible with an azeotrope of 58% deionized water and 42% isopropanol (Fisher Scientific, Fair Lawn, NJ) by volume. Because Nafion swells when saturated, and the amount of swelling is a function of ionic strength, the porosity had to be measured for each salt concentration used. Porosity was measured by injecting vegetable oil into the top of the presaturated flow column, which displaced the higher density isopropanol/water azeotrope downward. After preliminary confirmation that such displacement did not affect Nafion swelling, the porosity was calculated from the volume of vegetable oil required to displace the azeotrope from the pore space. The suspended colloids were carboxylate-modified polystyrene microspheres with diameter 106 nm (Seradyn, Indianapolis, IN), and refractive index 1.57, which remained stable in low ionic strength aqueous suspension. The suspension was mixed with a solution of magnesium chloride (Fisher Scientific, Fair Lawn, NJ) resulting in an ionic strength that exceeded the critical coagulation concentration (CCC), the ionic strength at which stable colloids first begin to aggregate, immediately before entry into the vertical column packed with the porous medium (Figure 2). The CCC was between 1.0 mM and 1.1 mM $MgCl_2$,

corresponding to ionic strength between 3.0 mM and 3.3 mM, determined by aggregate settling within a 24 h time frame (Table S1).

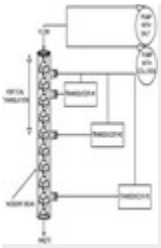

Figure 2. Schematic of filter column.

As colloid deposition progressed within the porous media, static light scattering (SLS) scans were acquired at different vertical positions by adjusting the column using a vertical stage controlled by LabVIEW. At each position, the intensity of scattered laser light was measured at 152 logarithmically spaced scattering angles from θ = 0.43° to 90°. Simultaneously, differential pressure measurements on variable reluctance transducers (Validyne, DP15, Northridge, CA) were taken across three distinct subsections of the column, from which permeability, k, was calculated from Darcy's law, then normalized by the clean bed permeability, k_0. Using the normalized permeability k/k_0 allows comparison of results obtained from different column packings, each of which will have a unique clean bed permeability, k_0. Specific deposit, σ, defined as the volume of deposited colloids divided by the total filter volume, was calculated as $\sigma = Cn/\rho$, where C is the colloid concentration [mg/L] in the pore space, n is porosity and ρ is the colloid density [mg/L]. Colloid concentration, in turn, was determined from the scattering intensity at approximately θ = 90° and a calibration curve constructed from known concentrations. Additional details on the filtration experiments are provided in Roth.(41)

A series of nine experiments was performed to investigate how deposit morphology and permeability varied with salt concentration, representing chemical effects, and flow rate, representing physical effects (Table 1). Specific discharge for the experiments varied between 19 m/d and 163 m/d. By comparison, most rapid sand filtration systems operate between 59 m/d and 233 m/d.(42) Logarithmically spaced discharge targets of 1.5, 3, 6, and 12 cm^3/min were established, but actual flow rates were confirmed by measuring volumes, which explains the slight deviation of the actual discharges from their targets. In order to observe variation with depth, measurements were taken in three vertically distinct regions of the column for each experiment (Figure 2). Measurements were taken during each of four different flow regimes: (1) early phase deposition in nearly clean porous media, (2) late-phase deposition in clogged porous media, (3) a no-flow phase with flow stopped, and finally (4) a flushing phase with a colloid-free solution eluted through the clogged sample. Flow rate and ionic strength were held constant for all four flow regimes in each experiment. The nine distinct experiments performed comprised 92 individual SLS scans. Of these, one experiment (9) was conducted with an ionic strength of 2.9 mM, just less than the CCC of 3.0–3.3 mM. In this experiment, the head loss was not significantly higher than the clean bed head loss, and scattering did not have a signal-to-noise ratio large enough to be detected. The apparent lack of aggregation and deposition in experiment 9 is consistent with the carboxylate-modified surfaces of the Seradyn microspheres used, because the carboxylate imposes a negative surface charge that causes good particle stability (i.e., repulsion). Accordingly, for this experiment, analysis of the SLS data revealed neither a fractal dimension nor a radius of gyration. Consequently, there will be no further discussion about the results from experiment 9.

Table 1. Overview of Clogging Experiments

Experiment	porosity	inlet colloid C [mg/L]	$MgCl_2$[mM]	ionic strength [mM]	specific discharge q [m/d]	velocity $v = q/n$ [m/d]	room temperature [°C]
1	0.26	33	16.3	49	19	74	21.0
2	0.26	64	16.2	49	36	138	21.1
3	0.26	131	16.0	48	76	292	21.4
4	0.26	130	16.0	48	149	574	20.9
5	0.26	130	8.0	24	153	588	23.4
6	0.22	132	4.0	12	151	692	22.4
7	0.11	131	2.0	6.0	134	1215	20.1
8	0.11	65	2.0	6.0	163	1468	23.1
9	0.05	133	0.98	2.9	150	3003	21.9

Optical oversaturation necessitated removal of low-angle data from most experiments, but this did not prevent collection of scattering data throughout all phases of each experiment, as shown in Tables S2–S3. A few experiments with high levels of colloid deposition lead to optical oversaturation, and these results were excluded from further analysis. This left 71 individual SLS scans, which were fitted to two scattering models (Figure 3) matching eq 2. The first model is a two-parameter model that fits a dimensionless scaling factor and the fractal dimension to the linear region of the plot of log(I) versus log(Q), where I is the normalized and background-subtracted intensity of scattered light and Q is the scattering wave vector.(43) The absolute value of the slope of this linear regression is equal to the fractal dimension, so the error of the fractal dimension was taken as the standard error of the slope. The second model is the three-parameter model of Teixeira(44) that additionally fits the radius of gyration to the full range of log(I) versus log(Q) data. The Akaike information criterion (AIC),(45) which accounts for the unequal number of parameters in these two models, was used to quantify each model's goodness-of-fit and consequently to identify the most appropriate model for each individual SLS scan. When the linear model fit better, indicated by a smaller AIC (i.e., a more negative number) no radius of gyration is reported (22 of 71 scans). For the remaining 59 scans, the Teixeira(44) model fit better, so both fractal dimension and radius of gyration are reported (59 of 71 scans). Details on data reduction, model fitting, and estimation of standard errors are provided in Roth et al.(40)

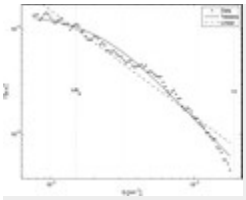

Figure 3. Static light scattering (SLS) data and models. Sample data are from experiment 7, middle position, during the no-flow phase after 274 pore volumes had been eluted, corresponding to the conceptual illustration in Figure 1c. The dashed line is the two-parameter model that determines the fractal dimension from the linear region of the log(*I*) – log(*Q*) plot. The solid line is the three-parameter model of Teixeira(44) that also determines the deposit radius of gyration, R_g. In this case, the three-parameter model has a smaller Akaike information criterion (AIC) and is therefore the model chosen for final consideration. Complete log(*I*) – log(*Q*) results and models, including fitted parameters, are provided in the Supporting Information (Figures S1–S92).

Results

The SLS curves obtained throughout the experiments agreed well with the theoretical functions developed to describe small-angle scattering from fractal aggregates, as shown in Figure 3, in Figures S1–S92, and as indicated by the typical root mean squared error of 0.054 log (base 10) units or less. To our knowledge, these measurements are the first in situ studies of deposit structure during a real-time clogging experiment. These data support the concept that colloid deposits can be characterized by a fractal dimension. Conversely, when a stable suspension was added (experiment 9), there was no clogging and no detectable fractal aggregate formation.

A key finding of this research is that permeability, colloid deposition, and deposit morphology (i.e., fractal dimension and radius of gyration) evolved in an orderly manner as each experiment progressed. This is notable because clear and repeatable trends signal the action of underlying mechanisms and hence the potential for development of a predictive model. To define these trends, Figure 4 shows the time evolution of normalized permeability (k/k_o), specific deposit (σ), fractal dimension (*D*), and radius of gyration (R_g) for typical experiments 5 and 7, where experiment 7 had lower porosity, lower ionic strength, and higher velocity than experiment 5.

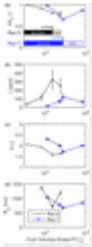

Figure 4. Clogging, accumulation, and deposit morphology versus pore volumes eluted for data collected at the middle position of high salinity, low velocity experiment 5 (8.0 mM $MgCl_2$, v = 588 m/d) and low salinity, high velocity experiment 7 (2.0 mM $MgCl_2$, v = 1215 m/d). (a) Normalized permeability, k/k_o. (b) Specific deposit, σ. (c) Colloid deposit fractal dimension, *D*. (d) Colloid deposit radius of gyration, R_g. The horizontal bars in (a) show the duration of the deposition, no-flow, and flushing phases of each experiment. For experiment 7, conceptual illustrations of deposit morphology are shown in Figure 1, and the raw data with fitted models at 274 pore volumes are shown in Figure 3. For all experiments, the Supporting Information provides tabulated results (Tables S2–S3) and raw data with fitted models (Figures S1–S92). The trends shown here were typical in most experiments (Table 2).

Injecting destabilized colloids caused a decrease in permeability (Figure 4a) and an increase in the specific deposit (Figure 4b). These trends were partially reversed when colloid-free fluid was introduced to the system during the flushing phase. However, the flushing phase did not restore all of the initial permeability nor remove all of the deposited colloids, indicating that deposition was at least partly irreversible. Deposit morphology manifests clear and repeatable trends, with both fractal dimension and radius of gyration starting relatively high at the early deposition phase, then getting smaller as deposition continues until a minimum is reached for the no flow measurements. Fractal dimension and radius of gyration then increase after flushing with a colloid-free solution. To facilitate discussion of these observations, we define a full trend as data that evolve as shown in Figure 4 through each flow regime (early deposition, late deposition, no flow, and flushing); we define an initial trend as data that follow Figure 4 only through early deposition, late deposition, and no flow. Examination of the results in Tables S2–S3 reveals that the majority of fractal dimension observations (54%) followed the full trend, while nearly all observations (80%) followed at least the initial trend (Table 2). The majority of observations (67%) of radius of gyration also followed the full trend shown in Figure 4d, with a larger proportion (78%) following at least the initial trend (Table 2).

Table 2. Trends in Fractal Dimension (*D*) and Radius of Gyration (R_g). Run 9 Was Omitted Because It Had Negligible Colloid Deposition

	initial trend[a]	full trend[b]
	Fractal Dimension (Figure 4c)	
all experiments	80%	54%
omit experiments 7–8	100%	75%
	Radius of Gyration (Figure 4d)	
all experiments	78%	67%
omit experiments 7–8	69%	43%

a Initial trends are defined as trends in the deposition and no flow phases.
b Full trends are defined as trends for all flow phases including the flushing phase.

We performed statistical analysis of the correlations between measured variables, finding that normalized permeability k/k_0 had a positive correlation with fractal dimension. That is, clogging (i.e., smaller k/k_0) was associated with low-fractal dimension colloid deposits, consistent with expectations for initially clean porous media.(9) Figure 5 summarizes plots of normalized permeability, k/k_0, versus fractal dimension, D, for data acquired at the middle vertical position of the column and spanning the full range of velocities (74–1468 m/d). Normalized permeability had a positive correlation with fractal dimension, with the R^2 values for linear regression near unity. Normalized permeability had a negative correlation with specific

deposit, with 5 of 7 linear regressions having $R^2 > 0.9$. That is, clogging was associated with larger specific deposits as expected. Weaker correlation between clogging and radius of gyration was also observed.

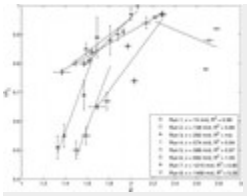

Figure 5. Normalized permeability, k/k_o, versus deposit fractal dimension, D, for various velocities, recorded at the middle flow cell position between transducers 1 and 2 on Figure 2.

The trends illustrated by Figure 5 were repeated, slightly less clearly, for the other vertical positions shown in Figure 2. Considering the data from all three flow cell positions, there is evidence of a velocity above which the positive correlation between normalized permeability and fractal dimension breaks down. For slower velocities, below 690 m/d, 9 out of 10 normalized permeability versus fractal dimension correlations had $R^2 > 0.9$. In contrast, for almost all experiments with faster velocities, no strong correlations were observed between normalized permeability and fractal dimension, suggesting an upper limit to the usefulness of fractal dimension as a metric for deposit morphology.

The data acquired during the no flow phase allowed comparison of deposit morphology as a function of distance from the inlet position for the experiments shown on Table S5. With the flow stopped, it was possible to measure deposit morphology at a snapshot in time. Specific deposit was highest near the inlet and always decreased with proximity to the outlet. However, in contrast to the trends with time summarized on Table 2, there were no discernible trends with distance for clogging, fractal dimension, or radius of gyration.

The data acquired during the flushing phase provided information on the structures of the aggregates that remained in the column once a mobile portion has been eluted. As shown in Figure 6, there is a marked increase in the fractal dimension when the velocity exceeds 690 m/d indicating that faster flow caused greater restructuring.

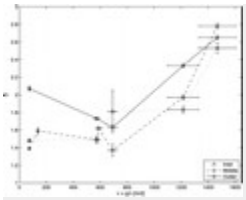

Figure 6. Deposit fractal dimension, D, versus velocity, v, measured during the flushing phase of each experiment, during which the influent colloid concentration was zero and the velocity matched that of the deposition phase. Note the shift in behavior above 690 m/d, which also corresponds to successively decreasing ionic strength (Table 1).

Discussion

A key finding of this work is evidence of a positive correlation between normalized permeability and fractal dimension, at least below velocities of 690 m/d. Clogging was equally associated with a lower fractal dimension and a higher specific deposit, and to a lesser degree with a smaller radius of gyration. These findings provide empirical support for the conclusion by Wiesner, (19) Mays,(9)and Ghezzehei(4) that fractal dimension could be a critical aspect of clogging by colloids in porous media.

Mechanism Linking Deposit Morphology and Clogging

The repeatable trends in permeability, specific deposit, and deposit morphology suggest the following conceptual model of colloidal processes during transport, deposition and flushing. Based on early measurements within the column near the inlet, the initial aggregates, formed by the addition of salt to the colloidal suspension immediately before entry into the flow cell, are relatively large and compact, with high D and R_g. Upon entry into the column, these aggregates are filtered by the porous media, reducing permeability as they deposit within the pore space. Deposition leads to higher fluid shear forces, which restructures and breaks up the aggregates. The products of the shear forces are smaller fragments of the initial aggregates, which would be dendritic in form according to this conceptual model. These lower-fractal-dimension products either protrude outward from the original deposit into the pore space or are released into suspension, both of which would impede flow. During the flushing phase, the fragments are preferentially removed from the column, leaving behind large, more compact deposits that are nevertheless significantly altered relative to the initial aggregates. Since ionic strength is held constant for all flow phases, including flushing, it is assumed that the ejected low-D, low-R_g fragments were in suspension. Under this possible deposition scenario, reductions in permeability are appreciably a function of the radius of gyration and fractal dimension of the initial deposits, with a significant dependence on the amount of fluid shear to which the deposits have been subjected.

Figure 1 shows a graphic representation of the evolution of aggregate morphology consistent with the results from the midcolumn scan position for experiment 7. The aggregate models were generated using an aggregation simulation code(46) constrained by experimental measurements of D and R_g obtained at 4 time points during the experiment. The code cannot generate models of colloidal deposits (i.e., aggregates of particles on a two-dimensional surface) and thus the images of Figure 1 serve as a qualitative description of morphology evolution.

Hydrodynamics and Geochemistry

The results reported here show the simultaneous effects of velocity (i.e., hydrodynamics) and ionic strength (i.e., geochemistry) on colloid deposit morphology. The fractal dimension of colloid deposits varies with velocity (Figure 6) and, to a lesser degree, with ionic strength (Figure 7), with the important caveat that the ionic strength must be sufficiently higher than the CCC to ensure rapid aggregation. As velocity increases to values beyond 690 m/d (Figure 6), deposit fractal dimension increases as well, reflecting a transition to more ballistic deposits with larger fractal dimensions.(47) The results reported here echo the observations of Veerapaneni and Wiesner,(15) who measured colloid deposit fractal dimension using SLS ex situ after resuspending frozen deposits extracted destructively. In particular, they reported fractal dimension D versus specific discharge q from 0.001 to 1 cm/s, corresponding to Peclet numbers from 1×10^3 to 2×10^5 for their experimental conditions. They reported decreasing D at lower q, which they attributed to the formation of compact columnar structures, and increasing D at higher q, which they attributed to deposit compaction by shear. These results are qualitatively similar to those shown in Figure 6, which correspond to higher Peclet numbers of 4×10^5 to 4×10^6, assuming the geometric mean diameter of swollen Nafion is five times its diameter when dry. Both studies clearly show that colloid deposit morphology depends on fluid velocity. However, in contrast to Veerapaneni and Wiesner's pioneering study, our results also include colloid deposit radius of gyration, which imposes an important additional constraint on the possible range of deposit morphology.

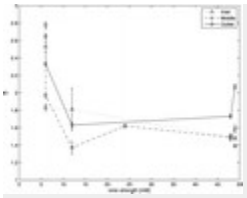

Figure 7. Deposit fractal dimension, *D*, versus ionic strength for the flushing phase of each experiment. Note, experiments with ionic strengths less than 50 mM all have a specific discharge of approximately 150 m/d, while those conducted at 50 mM have variable specific discharge (Table 1).

As ionic strength increases from 6 mM to 12 mM, deposit fractal dimension decreases, and then remains approximately constant with additional ionic strength (Figure 7). This initial decrease in fractal dimension is consistent with visual observations of colloid aggregation during determination of the CCC (Table S1), which showed a transition from kinetic to instantaneous aggregation with increasing ionic strength. Specifically, for ionic strengths between 1.1 and 15.0 mM, colloids aggregated within 24 h, but not immediately, indicating a transition from more rate-limited aggregation at lower ionic strengths with larger fractal dimensions to more diffusion-limited aggregation at higher ionic strengths with smaller fractal dimensions. Similar decreases in aggregate fractal dimension have been reported for zinc oxide nanoparticles with increasing ionic strength,(26) and for titanium dioxide nanoparticles with increasing pH.(25) For experiments 7 and 8 the ionic strength was above the CCC, but not high enough to induce immediate aggregation, which could explain why these experiments were the only instances that did not follow the initial trend of fractal dimension versus time (Table 2). These observations suggest that the dependence of deposit morphology on ionic strength can be thought of as a gradual transition rather than a binary switch. Much like the transition from laminar flow to turbulence, there appears to be a transition zone as ionic strength increases beyond the CCC in which deposit morphology varies.

Filtration Effects

Observations during the no flow phase (Figures 6-7), in which the entire flow column could be considered concurrently, suggest that aggregate passage through the porous media had little effect on the ultimate morphology of deposited aggregates. If physicochemical filtration affected deposit morphology, it would be expected that the fractal dimension or radius of gyration would evolve as a function of depth into the porous media. Specific deposit always decreased with increasing depth into the column, as predicted by classical filtration theory.(42) However, in opposition to filtration research of the past, (13, 14) permeability did not always increase with increasing depth into the column, even with the decreased specific deposit. Two instances of this can be seen in Table S5 for experiments 4 and 8, with due attention given to the relatively large standard error of the specific deposit. Comparing the middle to outlet position of experiment 4 and the inlet to middle position of experiment 8 during no flow, k/k_o slightly decreases even in the presence of a slightly decreasing specific deposit. A stronger example can be seen for experiment 6 during the transition from early deposition flow to late deposition flow, when specific deposit increased from 28 ± 10 ppm to 244 ± 84 ppm while normalized permeability increased from 0.83 ± 0.01 to 0.89 ± 0.01 (Table S3). These few examples add further support to the idea that deposit morphology is a controlling variable.

Limitations and Future Work

One limitation of the SLS method is that it cannot differentiate between material affixed to surfaces and transient aggregates carried in suspension. However, as most of the material is not removed by flushing, it appears that it is mostly surface-

associated. To further evaluate the proposed conceptual model for colloid deposition and clogging, it may be necessary to develop a nondestructive imaging technique, such as X-ray microtomography,(6, 7, 11) with sufficient resolution to fully determine the three-dimensional structure of colloid deposits within porous media (i.e., voxel resolution <50 nm). Until such measurements are feasible, however, our experiments have provided clear evidence that a nonrandom process is taking place and that deposit fractal dimension can be considered as a fundamental aspect of deposit morphology to be considered for further research. By discovering how colloid deposit morphology evolves and how these deposits affect other processes, it is hoped that the dynamics linking colloids, fluids, and porous media can be linked through a more fundamental, mechanistic model.

Supporting Information

The authors declare no competing financial interest.

Acknowledgment

We received constructive feedback from three anonymous referees, one of whom provided extensive comments that thoroughly improved the manuscript. This research was supported by the U.S. Department of Energy, Subsurface Biogeochemistry Research Program (award DE-SC0006962). B.G. was supported as part of the Subsurface Science Scientific Focus Area funded by the U.S. Department of Energy, Office of Science, Office of Biological and Environmental Research (award DE-AC02-05CH11231).

References

This article references 47 other publications.

1. Kozeny, J. Über Kapillare Leitung des Wassers im Boden *Sitzungsber Akad. Wiss., Wien* **1927**, 136 (2a)271– 306
2. Carman, P. C. Fluid Flow through Granular Beds *Trans. Inst. Chem. Eng.* **1937**, 15, 150
3. Xu, P.; Yu, B. M. Developing a new form of permeability and Kozeny-Carman constant for homogeneous porous media by means of fractal geometry *Adv. Water Resour.* **2008**, 31 (1) 74– 81 DOI: 10.1016/j.advwatres.2007.06.003
4. Ghezzehei, T. A. Linking sub-pore scale heterogeneity of biological and geochemical deposits with changes in permeability *Adv. Water Resour.* **2012**, 39, 1– 6 DOI: 10.1016/j.advwatres.2011.12.015
5. Chamberlain, E. J.; Gow, A. J. Effect of Freezing and Thawing on the Permeability and Structure of Soils*Eng. Geol.* **1979**, 13 (1–4) 73– 92 DOI: 10.1016/0013-7952(79)90022-X
6. Armstrong, R.; Ajo-Franklin, J. Investigating biomineralization using synchrotron based X-ray computed microtomography *Geophys. Res. Lett.* **2011**, 38, L08406 DOI: 10.1029/2011GL046916
7. Chen, C.; Lau, B.; Gaillard, J. F.; Packman, A. I. Temporal evolution of pore geometry, fluid flow, and solute transport resulting from colloid deposition *Water Resour. Res.* **2009**, 45, W06416 DOI: 10.1029/2008WR007252
8. Coughlin, J. P.; Campbell, C. D.; Mays, D. C. Infiltration and Clogging by Sand and Clay in a Pervious Concrete Pavement System *J. Hydrol Eng.* **2012**, 17 (1) 68– 73 DOI: 10.1061/(ASCE)HE.1943-5584.0000424
9. Mays, D. C. Contrasting clogging in granular media filters, soils, and dead-end membranes *J. Environ. Eng.***2010**, 136 (5) 475– 480 DOI: 10.1061/(ASCE)EE.1943-7870.0000173

10. Mays, D. C., Clogging in managed aquifer recharge: Flow, geochemistry, and clay colloids. In *Clogging Issues Associated with Managed Aquifer Recharge Methods*; Martin, R., Ed.; International Association of Hydrogeologists: Australia, **2013**; pp 14– 24.
11. Menon, M.; Yuan, Q.; Jia, X.; Dougill, A. J.; Hoon, S. R.; Thomas, A. D.; Williams, R. A. Assessment of physical and hydrological properties of biological soil crusts using X-ray microtomography and modeling *J. Hydrol.* **2011**, 397 (1–2) 47– 54 DOI: 10.1016/j.jhydrol.2010.11.021
12. Krauss, E. D.; Mays, D. C. Modification of the Kozeny-Carman Equation To Quantify Formation Damage by Fines in Clean, Unconsolidated Porous Media *SPE Reserv. Eval. Eng*. **2014**, 17 (4) 466– 472 DOI: 10.2118/165148-PA
13. Mays, D. C.; Hunt, J. R. Hydrodynamic aspects of particle clogging in porous media *Environ. Sci. Technol*.**2005**, 39 (2) 577– 584 DOI: 10.1021/es049367k
14. Mays, D. C.; Hunt, J. R. Hydrodynamic and chemical factors in clogging by montmorillonite in porous media*Environ. Sci. Technol.* **2007**, 41 (16) 5666– 5671 DOI: 10.1021/es062009s
15. Veerapaneni, S.; Wiesner, M. R. Deposit morphology and head loss development in porous media *Environ. Sci. Technol*. **1997**, 31 (10) 2738– 2744 DOI: 10.1021/es960979h
16. Mandelbrot, B. *The Fractal Geometry of Nature*; W.H. Freeman and Company: New York, **1982**.
17. Bushell, G. C.; Yan, Y. D.; Woodfield, D.; Raper, J.; Amal, R. On techniques for the measurement of the mass fractal dimension of aggregates *Adv. Colloid Interface Sci.* **2002**, 95 (1) 1– 50 DOI: 10.1016/S0001-8686(00)00078-6
18. Sorensen, C. M. Q-space analysis of scattering by particles: A review *J. Quant. Spectrosc. Radiat. Transfer***2013**, 131, 3– 12 DOI: 10.1016/j.jqsrt.2012.12.029
19. Wiesner, M. R. Morphology of particle deposits *J. Environ. Eng.* **1999**, 125 (12) 1124– 1132 DOI: 10.1061/(ASCE)0733-9372(1999)125:12(1124)
20. Kretzschmar, R.; Borkovec, M.; Grolimund, D.; Elimelech, M. Mobile subsurface colloids and their role in contaminant transport *Adv. Agron.* **1999**, 66, 121– 193 DOI: 10.1016/S0065-2113(08)60427-7
21. Molnar, I. L.; Johnson, W. P.; Gerhard, J. I.; Willson, C. S.; O'Carroll, D. M., Predicting colloid transport through saturated porous media: A critical review. *Water Resour. Res.* **2015**, 51, DOI: DOI: 10.1002/2015WR017318 .
22. Ryan, J. N.; Elimelech, M. Colloid mobilization and transport in groundwater *Colloids Surf., A* **1996**, 107, 1–56 DOI: 10.1016/0927-7757(95)03384-X
23. Tufenkji, N. Modeling microbial transport in porous media: Traditional approaches and recent developments*Adv. Water Resour.* **2007**, 30, 1455– 1469 DOI: 10.1016/j.advwatres.2006.05.014
24. Lin, S. H.; Wiesner, M. R. Deposition of Aggregated Nanoparticles - A Theoretical and Experimental Study on the Effect of Aggregation State on the Affinity between Nanoparticles and a Collector Surface *Environ. Sci. Technol*. **2012**, 46 (24) 13270– 13277 DOI: 10.1021/es3041225
25. Chowdhury, I.; Walker, S. L.; Mylon, S. E. Aggregate morphology of nano-TiO2: role of primary particle size, solution chemistry, and organic matter *Environ. Sci-Proc. Imp* **2013**, 15 (1) 275– 282 DOI: 10.1039/C2EM30680H
26. Jassby, D.; Budarz, J. F.; Wiesner, M. Impact of Aggregate Size and Structure on the Photocatalytic Properties of TiO2 and ZnO Nanoparticles *Environ. Sci. Technol.* **2012**, 46 (13) 6934– 6941 DOI: 10.1021/es202009h
27. Legg, B. A.; Zhu, M. Q.; Comolli, L. R.; Gilbert, B.; Banfield, J. F. Impacts of Ionic Strength on Three-Dimensional Nanoparticle Aggregate Structure and Consequences for Environmental Transport and Deposition *Environ. Sci. Technol*. **2014**, 48 (23) 13703– 13710 DOI: 10.1021/es502654q
28. Lattuada, M. Retarded hydrodynamic properties of fractal clusters *J. Colloid Interface Sci.* **2014**, 429, 8– 16DOI: 10.1016/j.jcis.2014.05.003
29. Xu, N.; Fan, L. Numerical simulation of flow involving a fractal aggregate *J. Taiwan Inst. Chem. Eng*. **2014**,45 (4) 1403– 1410 DOI: 10.1016/j.jtice.2014.03.013

30. Fellay, L. S.; Twist, C.; Vanni, M. Motion of rigid aggregates under different flow conditions *Acta Mech.* **2013**,224 (10) 2225– 2248 DOI: 10.1007/s00707-013-0928-9
31. Li, X.; Huang, H.; Meakin, P. Level set simulation of coupled advection-diffusion and pore structure evolution due to mineral precipitation in porous media *Water Resour. Res.* **2008**, 44, W12407 DOI: 10.1029/2007WR006742
32. Thullner, M.; Mauclaire, L.; Schroth, M. H.; Kinzelbach, W.; Zeyer, J. Interaction between water flow and spatial distribution of microbial growth in a two-dimensional flow field in saturated porous media *J. Contam. Hydrol.* **2002**, 58 (3–4) 169– 189 DOI: 10.1016/S0169-7722(02)00033-5
33. Englert, A.; Hubbard, S. S.; Williams, K. H.; Li, L.; Steefel, C. I. Feedbacks Between Hydrological Heterogeneity and Bioremediation Induced Biogeochemical Transformations *Environ. Sci. Technol.* **2009**, 43(14) 5197– 5204 DOI: 10.1021/es803367n
34. Veerapaneni, S.; Wiesner, M. R. Particle Deposition on an Infinitely Permeable Surface - Dependence of Deposit Morphology on Particle-Size *J. Colloid Interface Sci.* **1994**, 162 (1) 110– 122 DOI: 10.1006/jcis.1994.1015
35. Wang, J.; Pan, S. R.; Luo, D. P. Characterization of cake layer structure on the microfiltration membrane permeability by iron pre-coagulation *J. Environ. Sci.* **2013**, 25 (2) 308– 315 DOI: 10.1016/S1001-0742(12)60025-4
36. Cai, J.; Lu, N.; Sorensen, C. M. Comparison of Size and Morphology of Soot Aggregates as Determined by Light-Scattering and Electron-Microscope Analysis *Langmuir* **1993**, 9 (11) 2861– 2867 DOI: 10.1021/la00035a023
37. Schaefer, D. W.; Martin, J. E.; Wiltzius, P.; Cannell, D. S. Fractal Geometry of Colloidal Aggregates *Phys. Rev. Lett.* **1984**, 52 (26) 2371– 2374 DOI: 10.1103/PhysRevLett.52.2371
38. Wakamatsu, T. Method and apparatus for characterization of electric field-induced aggregation in pre-crystalline protein solutions *Rev. Sci. Instrum.* **2015**, 86 (1) 015112 DOI: 10.1063/1.4906328
39. Mays, D. C.; Cannon, O. T.; Kanold, A. W.; Harris, K. J.; Lei, T. C.; Gilbert, B. Static light scattering resolves colloid structures in index-matched porous media *J. Colloid Interface Sci.* **2011**, 363, 418– 424 DOI: 10.1016/j.jcis.2011.06.046
40. Roth, E. J.; Mont-Eton, M. E.; Gilbert, B.; Lei, T. C.; Mays, D. C. Measurement of colloidal phenomena during flow through refractive index matched porous media. Rev. Sci. Instrum. **2015**, (under review).
41. Roth, E. J. Linking Colloid Deposit Morphology and Clogging: Insights by Measurement of Deposit Fractal Dimension. M.S. thesis, Department of Civil Engineering, University of Colorado Denver, Denver, CO, **2013**.
42. MWH, *Water Treatment: Principles and Design*, 2 ed.; Chapter 11; John Wiley and Sons, Inc.: Hoboken, NJ,**2005**.
43. Sorensen, C. M. Light scattering by fractal aggregates: A review *Aerosol Sci. Technol.* **2001**, 35 (2) 648–687 DOI: 10.1080/02786820117868
44. Teixeira, J. Small-angle scattering by fractal systems *J. Appl. Crystallogr.* **1988**, 21, 781– 785 DOI: 10.1107/S0021889888000263
45. Kutner, M. H.; Nachtsheim, C. J.; Neter, J.; Li, W. *Applied Linear Statistical Models*, Chapter 9; McGraw-Hill/Irwin: New York, **2005**.
46. Wozniak, M.; Onofri, F. R. A.; Barbosa, S.; Yon, J.; Mroczka, J. Comparison of methods to derive morphological parameters of multi-fractal samples of particle aggregates from TEM images *J. Aerosol Sci.***2012**, 47, 12– 26 DOI: 10.1016/j.jaerosci.2011.12.008
47. Elimelech, M.; Gregory, J.; Jia, X.; Williams, R. A. *Particle Deposition and Aggregation*; Butterworth-Heinemann: Boston, **1995**; p 441.